# Theoretical photoionization spectra for the Mg-like $S^{4+}$ ion: Partial and total cross sections for the ground $3s^2\ ^1S$ and excited $3s3p\ ^3P$ and $3s3p\ ^1P$ states

Dae-Soung Kim*
*Department of e-Business, Gyeonggi College of Science and Technology, Siheung, Jungwang-Dong 2121-3, Gyonggi-Do 429-792, Republic of Korea*

Duck-Hee Kwon†
*Nuclear Data Center, Korea Atomic Energy Research Institute, Daejeon 305-600, Republic of Korea*
(Received 6 August 2013; published 30 September 2013)

The partial and total photoionization cross sections of the Mg-like $S^{4+}$ ion for the ground $3s^2\ ^1S^e$ and the excited $3s3p\ ^3P^o$ and $3s3p\ ^1P^o$ initial states, leaving the residual $S^{5+}$ $3l$ states, have been calculated in both the dipole length and velocity forms using a noniterative eigenchannel $R$-matrix method combined with multichannel quantum-defect theory at the $R$-matrix surface. Noticeable features in the cross sections are found for the autoionizing Rydberg series converging to the $S^{5+}$ $3l$ thresholds, owing to the effect of interlopers which converge to the other threshold limits. The resonance parameters for low members of these autoionizing levels are identified and characterized. Our calculational results are compared with the available previous results, and the ionization thresholds are in better agreement with NIST data than Opacity Project (OP) results. The present photoionization cross sections are in overall agreement with the OP results, but some discrepancies are found.

DOI: 10.1103/PhysRevA.88.033426 PACS number(s): 32.80.Fb, 32.80.Zb

## I. INTRODUCTION

Photoionization is a fundamental atomic process that plays important roles in many physical systems, including a broad range of astrophysical objects. Especially, the recent investigation of sulfur abundance in the atmosphere of old galactic stars has been performed precisely by Spite *et al.* [1]. Photoionization of Mg atom and Mg-like ions is also important in astrophysical plasmas exposed to hot sources of radiation. Therefore, photoionization cross sections are required to model such systems and it is an important task for the atomic physics community to provide the data.

After the first theoretical study of photoionization cross section of a Mg atom by Bates and Altic in 1973 [2], the properties of Mg and Mg-like ions have attracted a great deal of attention theoretically [3–21]. Specifically, the Opacity Project (OP) team [19–21] which was formed in 1984 to calculate the extensive atomic data required to estimate stellar envelope opacities and other related quantities, has performed many remarkable works. Experimental investigations of the autoionizing resonance series for the Mg atom started as early as 1969 by Mehlman-Balloffet and Esteva [22]. Other high-resolution experiments including the Mg-like ions have been followed up with quantitative studies [23–28].

In the present article, we report the partial and total cross sections for the photoionization of the Mg-like $S^{4+}$ ion for photon energy ranges from the $S^{5+}$ $3s$ threshold up to the $S^{5+}$ $4s$ threshold, using the variational $R$-matrix method [14]. We have considered the following photoionization processes,

$$\begin{aligned} S^{4+}(3s^2)^1S^e + \hbar\omega &\rightarrow S^{4+*}(3lnl')^1P^o \\ &\searrow [S^{5+}(3l) + e^-(\epsilon l')]^1P^o, \end{aligned}$$

$$\begin{aligned} S^{4+}(3s3p)^{3,1}P^o + \hbar\omega &\rightarrow S^{4+*}(3lnl')^{3,1}S^e, P^e, D^e \\ &\searrow [S^{5+}(3l) + e^-(\epsilon l')]^{3,1}S^e, P^e, D^e, \end{aligned}$$

where $\hbar\omega$ represents the incident photon energy and $S^{4+*}(3lnl')$ ($n \geqslant 3$) are taken into account as possible autoionizing intermediate doubly excited states.

Since there are no previous experimental data to compare with, our calculational results will be compared with those of OP results. Even though plasma spectroscopy is a source of high-resolution data for the experimental studies of these atomic and ionic systems, the different charge states obtained in the plasma and the large number of produced lines make the identification of spectroscopic levels difficult. However, since the utilization of a merged-photon-ion beam setup with synchrotron radiation from an undulator has enabled photoionization studies of the atomic and even ionic system [29–33], the identification of resonance structures for this Mg-like $S^{4+}$ ion is expected to be given in similar experiments.

With a brief description of the theoretical method used for the present calculation in the next section, the results are presented and discussed in Sec. III.

## II. THEORETICAL CALCULATIONS

The calculations are performed using the variational $R$-matrix method [34], which is the reformulation of the noniterative eigenchannel $R$-matrix method [4]. Neglecting relativistic effects, the Hamiltonian of the two valence electrons of the Mg-like $S^{4+}$ ion outside of the closed shell core can be written as

$$H = -\frac{1}{2}\nabla_1^2 - \frac{1}{2}\nabla_2^2 + U(r_1) + U(r_2) + \frac{1}{r_{12}}, \qquad (1)$$

where $U(r)$ describes the effective potential due to the interaction of each valence electron with the nucleus and inner shell core electrons. We have adopted a potential of

*dskim@gtec.ac.kr
†hkwon@kaeri.re.kr

 

TABLE I. Semiempirical parameters describing the model potential experienced by the valence electron in the $S^{4+}$ ion.

| Ion | $l$ | $\alpha_1^l$ | $\alpha_2^l$ | $\alpha_3^l$ | $r_c^l$ |
|---|---|---|---|---|---|
| $S^{4+}$ | 0 | 5.71074 | 7.10603 | 4.01821 | 0.35 |
| $\alpha_{cp} = 0.0721$ | 1 | 5.79539 | 7.29568 | 3.97712 | 0.35 |
| | 2 | 5.61063 | 6.76609 | 4.92866 | 0.35 |
| | $\geqslant 3$ | 5.78338 | 5.92456 | 6.04770 | 0.35 |

the form [35]

$$U(r) = -\frac{1}{r}\left[2 + (Z-2)e^{-\alpha_1^l r} + \alpha_2^l r e^{-\alpha_3^l r}\right] - \frac{\alpha_{cp}}{2r^4} \times \left[1 - e^{-(r/r_c^l)^6}\right], \quad (2)$$

where $Z$ is a nuclear charge. $\alpha_{cp}$ is the experimental dipole polarizability [36]. The parameters $\alpha_i^l$ and $r_c^l$ are chosen to optimize until the calculated energy eigenvalues obtained from the potential agree with the experimental energies of $S^{6+}$, and their values are given in Table I.

We represented both initial and final states by configuration-interaction wave functions. We use a basis $y_{nl}$ consisting of antisymmetrized products of one-electron orbitals $\phi_{nl}(r)Y_{lm}(\Omega)$ which are eigenfunctions of the one-electron Hamiltonian $-\frac{1}{2}\nabla^2 + U(r)$. The one-electron radial wave functions are closed $\phi_{nl}^c$ and open $\phi_{nl}^o$ types, depending on their behavior over the reaction surface [5]. We used 20 orbitals of $\phi_{nl}^c$ type which vanish on the boundary $r_0 = 12$ a.u., and two orbitals of $\phi_{nl}^o$ type which yield nonzero values on the boundary for each channel in our calculation. The final two-electron basis set used for photoionization of the ground $3s^2\ {}^1S^e$ state is listed in Table II. It should be noted that all closed orbitals are orthogonal to each other and the achieved average orthonormality $\langle\phi_i|\phi_j\rangle = \delta_{ij}$ at the present calculations is less than $10^{-12}$ for closed-type orbitals. The final two-electron basis set for photoionization of the excited $3s3p\ {}^{3,1}P^o$ initial states have been formed similarly.

The energy-normalized eigenstates $\psi_\alpha$ in each channel $i$ can be represented by a linear combination of the unnormalized $R$-matrix eigenstates $\psi_\beta = \sum_i c_i y_i$,

$$\psi_\alpha = \sum_{\beta,i} \psi_\beta (I^{-1})_{\beta i} U_{i\alpha} \cos(\pi\mu_\alpha), \quad (3)$$

where $U_{i\alpha}$ and $\mu_\alpha$ are the eigenvector elements and eigenquantum defects [37]. The details of formulation and notations related with the above eigenchannel wave functions are discussed by Greene and Jungen [37]. These variational wave functions are connected to the reduced dipole matrix elements in length form as

$$d_\alpha(L) = \langle\psi_\alpha\|\vec{r}_1 + \vec{r}_2\|\psi_0\rangle, \quad (4)$$

and in the velocity form as

$$d_\alpha(V) = \frac{1}{\omega}\langle\psi_\alpha\|\vec{\nabla}_1 + \vec{\nabla}_2\|\psi_0\rangle, \quad (5)$$

where $\psi_0$ represents the ground-state wave function. In most cases, the agreement between the length and velocity forms indicates the accuracy of the calculation.

TABLE II. Two-electron basis functions used for photoionization of the ground $3s^2\ {}^1S^e$ state of the $S^{4+}$ ion.

| Closed-type orbitals | Open-type orbitals |
|---|---|
| $nsmp$ | $nskp$ |
| $npms$ | $npks$ |
| $npmd$ | $npkd$ |
| $ndmp$ | $ndkp$ |
| $ndmf$ | $ndkf$ |
| $(3 \leqslant n \leqslant 22), (n \leqslant m \leqslant 22)$ | $(k = 23,24)$ |

### A. Cross section

In order to calculate partial and total photoionization cross sections, we need to find a new set of solutions $\psi_i(\epsilon)$ with $i = 1, \ldots, N_o$ from $\psi_\alpha$ which should remain well behaved as $r \to \infty$. The $N_o \times N_o$ open-channel reaction matrix is written as [37]

$$K_{\rm phys}^{oo} = K^{oo} - K^{oc}[K^{cc} + \tan\pi n^*]^{-1}K^{co}, \quad (6)$$

where the effective quantum number in the closed channels for this ionic system is given by

$$n^* = \frac{Z-N}{\sqrt{2(E_t - E_r)}}, \quad (7)$$

where $Z$ is the atomic number, $N$ is the number of electrons in the ion, $E_t$ is the threshold energy, and $E_r$ represents the corresponding resonance energy. The eigenphase in each channel $i$ is then defined as

$$\delta_i = \tan^{-1}\lambda_i, \quad i = 1, \ldots, N_o, \quad (8)$$

where $\lambda_i$ is the eigenvalue of $K_{\rm phys}^{oo}$. A resonance position $E_r$ may be defined as the energy at which the eigenphase sum $\delta$ has its maximum value of $d\delta/dE$. The width of the resonance $\Gamma_r$ is related to the inverse of the eigenphase gradient,

$$\Gamma_r = 2\left(\frac{d\delta}{dE}\right)^{-1}_{E=E_r}. \quad (9)$$

The associated dipole matrix element is given by

$$d_{\rm phys}^o = d_\alpha^o - d_\alpha^c[K^{cc} + \pi n^*]^{-1}K^{co}, \quad (10)$$

and the partial photoionization cross section is given by

$$\sigma_i = \frac{4\pi^2}{3(137)}\omega|d_i^{(-)}|^2 \quad (11)$$

in atomic units, where

$$d_i^{(-)} = \frac{d_{\rm phys}^o}{1 + iK_{\rm phys}^{oo}}. \quad (12)$$

Finally, the total photoionization cross section is given by

$$\sigma = \frac{4\pi^2}{3(137)}\omega\sum_i |d_i^{(-)}d_i^{(-)\dagger}|. \quad (13)$$

## III. RESULTS AND DISCUSSIONS

The calculated ionization energies (in eV) of the $S^{5+}$ $3l$ thresholds relative to the initial ground $^1S$ and excited $^{3,1}P$

TABLE III. Present ionization thresholds (in eV) relative to the ground and excited states of Mg-like $S^{4+}$.

| States | $3s\ ^2S$ | $3p\ ^2P$ | $3d\ ^2D$ | $4s\ ^2S$ |
|---|---|---|---|---|
| $3s^2\ ^1S^e$ | 72.365 | 85.596 | 103.044 | 117.372 |
| OP [21] | 72.669 | 85.805 | 102.790 | 117.365 |
| NIST [38] | 72.365 | 85.609 | 103.044 | 117.370 |
| $3s3p\ ^3P^o$ | 61.905 | 75.136 | 92.584 | 106.911 |
| OP [21] | 66.077 | 79.213 | 96.198 | 110.773 |
| NIST [38] | 61.978 | 75.222 | 92.657 | 106.983 |
| $3s3p\ ^1P^o$ | 56.847 | 70.078 | 87.526 | 101.854 |
| OP [21] | 56.698 | 69.834 | 86.819 | 101.394 |
| NIST [38] | 56.600 | 69.844 | 87.279 | 101.605 |

states of the Mg-like $S^{4+}$ ion are shown in Table III. The energies of the NIST data [38] listed in Table III have been averaged by $\sum_l (g_l E_l)/\sum_l g_l$ to compare with our results, where $g_l$ represents the statistical weight for the $l$ state. Our present results are in excellent agreement with the energies of the NIST data, however, there are some differences with the OP results [21] owing to the different calculational methods.

### A. Photoionization from the ground $3s^2\ ^1S$ state of Mg-like $S^{4+}$ ion

The photoionization cross sections leading to the ionic $S^{5+}$ $3s$, $3p$, and $3d$ states from the ground state of the Mg-like $S^{4+}$ ion have been calculated in the energy region from the first ionization threshold up to the $S^{5+}$ $4s$ threshold limit. First, the calculational results of the present partial photoionization cross sections from the ground state of the Mg-like $S^{4+}$ ion are shown in Fig. 1 as a function of photon energy. The good agreement between the length (black solid curve) and velocity (red dotted curve) results indicates the accuracy of the calculation.

The photoionization cross sections leading to the the $S^{5+}$ $3s$ state from the ground state of the Mg-like $S^{4+}$ ion are displayed in Fig. 1(a). In the energy region below the $S^{5+}$ $3p$ threshold, for the photoionization of the ground state of the $S^{4+}$ ion, only one open channel $3s\epsilon p$ is possible. Along with the $3s\epsilon p$ channel that opens at the first threshold, $3pns\ ^1P$ and $3pnd\ ^1P$ states ionize into the continuum states of $3p\epsilon s$ and $3p\epsilon p$ channels above the $S^{5+}$ $3p$ threshold. Thus, the photoionization process can branch to either $S^{5+}$ $3s$ or $3p$ final states. The partial cross sections $3p\epsilon s$ and $3p\epsilon d$ are shown in Figs. 1(b) and 1(c), respectively. These cross sections are fundamentally different from the $3s\epsilon p$ in one very important respect: Photoionization to $3s\epsilon p$ is eventually a single-electron $s \rightarrow p$ transition. Photoionization to the $S^{5+}$ $3p$ state, on the other hand, requires a true two-electron transition, i.e., photoionization plus excitation. This two-electron process is much less likely than a single-electron transition. As a result, it is expected that the $S^{5+}$ $3p$ cross sections $\sigma_{3p\epsilon s}\ ^1P$ and $\sigma_{3p\epsilon d}\ ^1P$ will be small compared to the $S^{5+}$ $3s$ cross section $\sigma_{3s\epsilon p}\ ^1P$. From Figs. 1(a)–1(c), it is evident that this is indeed the case. As photon energy increases to the energy region

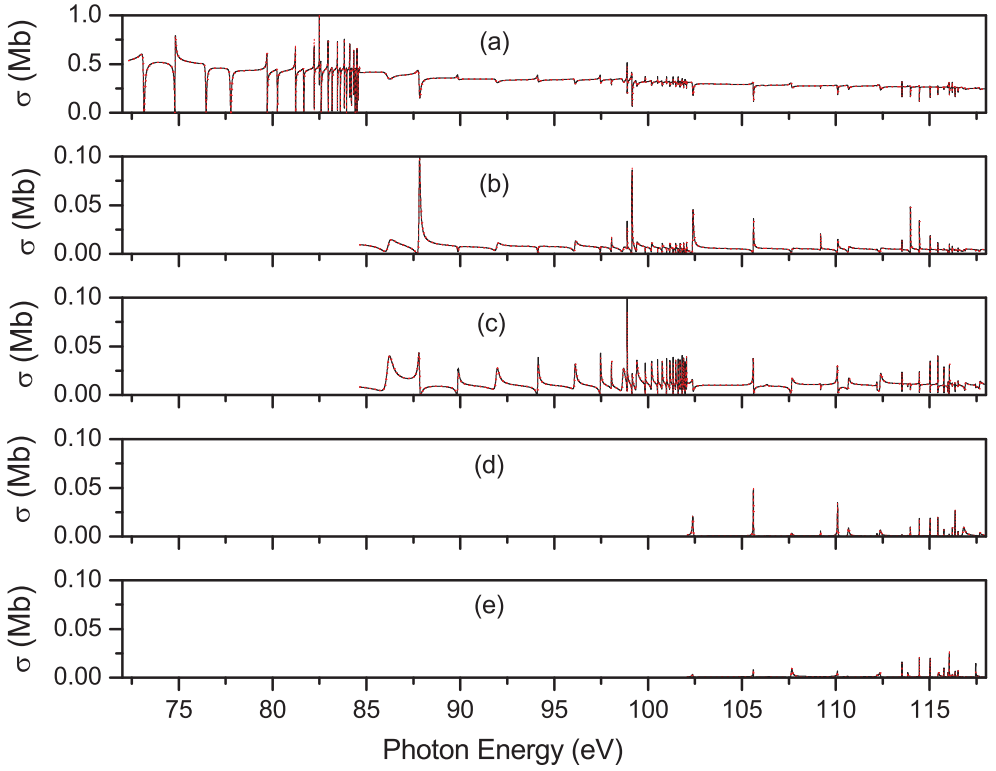


FIG. 1. (Color online) Partial photoionization cross sections for the processes $^1S^e \rightarrow\ ^1P$ of the Mg-like $S^{4+}$ ion in the energy range up to the $S^{5+}$ $4s$ threshold limit as a function of the photon energy: (a) cross sections $\sigma_{3s\epsilon p}\ ^1P$, (b) cross sections $\sigma_{3p\epsilon s}\ ^1P$, (c) cross sections $\sigma_{3p\epsilon d}\ ^1P$, (d) cross sections $\sigma_{3d\epsilon p}\ ^1P$, (e) cross sections $\sigma_{3d\epsilon f}\ ^1P$. The black solid and red dotted lines represent the present length and velocity results, respectively.

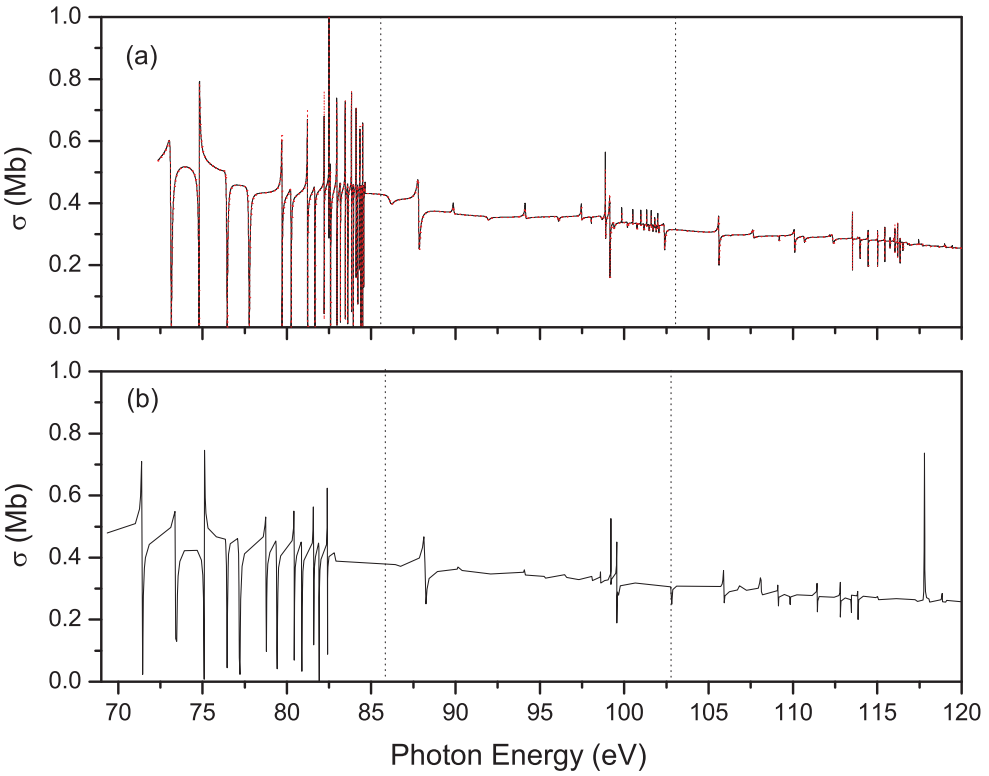


FIG. 2. (Color online) Photoionization cross sections from the ground-state of the Mg-like $S^{4+}$ ion in the energy range up to the $S^{5+}$ $4s$ threshold limit as a function of the photon energy: (a) Present length (black solid line) velocity results (red dotted), (b) OP results [21]. The vertical dotted lines represent the $S^{5+}$ $3p$ and $3d$ thresholds, respectively.

between the $S^{5+}$ $3d$ and $4s$ thresholds, the photoionization process can branch to the $S^{5+}$ $3s$, $3p$, and $3d$ channels. The present length and velocity forms of this $S^{5+}$ $3d$ cross section $\sigma_{3d\epsilon p}$ $^1P$ and $\sigma_{3d\epsilon f}$ $^1P$ are also shown in Figs. 1(d) and 1(e), respectively. The nonresonant background cross sections for these ionizations plus excitation are very small for the reasons discussed above.

The present length (black solid curve) and velocity (red dotted curve) results of total photoionization cross sections for the ground state of the Mg-like $S^{4+}$ $3s$ ion, the sum of all the individual partial cross sections of Fig. 1, are shown in Fig. 2(a), along with the OP results in Fig. 2(b) [21].

As shown in Fig. 2, our present results of the total photoionization cross section for the ground state of the Mg-like $S^{4+}$ ion are in overall agreement with the OP results [21]. While the database of OP results [21] contains the photoionization cross sections for almost all states of many atoms or ions, most of them do not have enough tiny energy points. On the other hand, we have used the equal tiny energy intervals $\Delta E = 0.002$ eV in the calculations. Thus, our results represent richer resonance structures than the OP results. The slight shift of the resonance structure is due to the difference in the threshold energies in the two calculations as given in Table III.

In the energy region below the $S^{5+}$ $3p$ threshold, there are two Rydberg series, $3pns$ $^1P$ and $3pnd$ $^1P$ ($n \geqslant 6$), converging to the $S^{5+}$ $3p$ threshold. However, the interloper $4s5p$ $^1P$ resonance converging to the $S^{5+}$ $4s$ threshold has an effect on the $3p9s$ $^1P$ resonance as shown in Table IV. These resonances appear to have a high degree of asymmetry (a Fano profile of about $q = 1$) so that their integrated effect

TABLE IV. Effective quantum number ($n^*$), position ($E_r$ in eV), and width ($\Gamma_r$ in eV) of resonances converging to the $S^{5+}$ $3l$ thresholds, which are owing to the photoionization processes $^1S \rightarrow {}^1P^o$.

| | $^1P^o$ | | | | $^1P^o$ | | |
|---|---|---|---|---|---|---|---|
| $3pns$ | $n^*$ | $E_r$ | $\Gamma_r$ | $3pnd$ | $n^*$ | $E_r$ | $\Gamma_r$ |
| 6 | 5.226 | 73.141 | 0.248 | 6 | 5.614 | 74.804 | 0.087 |
| 7 | 6.101 | 76.458 | 0.204 | 7 | 6.592 | 77.769 | 0.238 |
| 8 | 7.603 | 79.712 | 0.056 | 8 | 7.980 | 80.254 | 0.079 |
| 9 | | | | 9 | 8.822 | 81.225 | 0.034 |
| 10 | 9.298 | 81.661 | 0.046 | 10 | 10.034 | 82.217 | 0.007 |
| $3dnp$ | $n^*$ | $E_r$ | $\Gamma_r$ | $3dnf$ | $n^*$ | $E_r$ | $\Gamma_r$ |
| 4 | 3.373 | 73.141 | 0.249 | 4 | 4.078 | 82.587 | 0.059 |
| 5 | 4.502 | 86.261 | 1.491 | 5 | 5.081 | 89.869 | 0.212 |
| 6 | 5.533 | 91/933 | 0.579 | 6 | 6.178 | 94.131 | 0.172 |
| 7 | | | | 7 | 7.000 | 96.103 | 0.296 |
| 8 | 7.807 | 97.464 | 0.098 | 8 | 8.252 | 98.048 | 0.049 |
| 9 | 8.825 | 98.676 | 0.438 | 9 | 9.048 | 98.889 | 0.012 |
| 10 | 9.640 | 99.383 | 0.190 | 10 | 10.322 | 99.852 | |

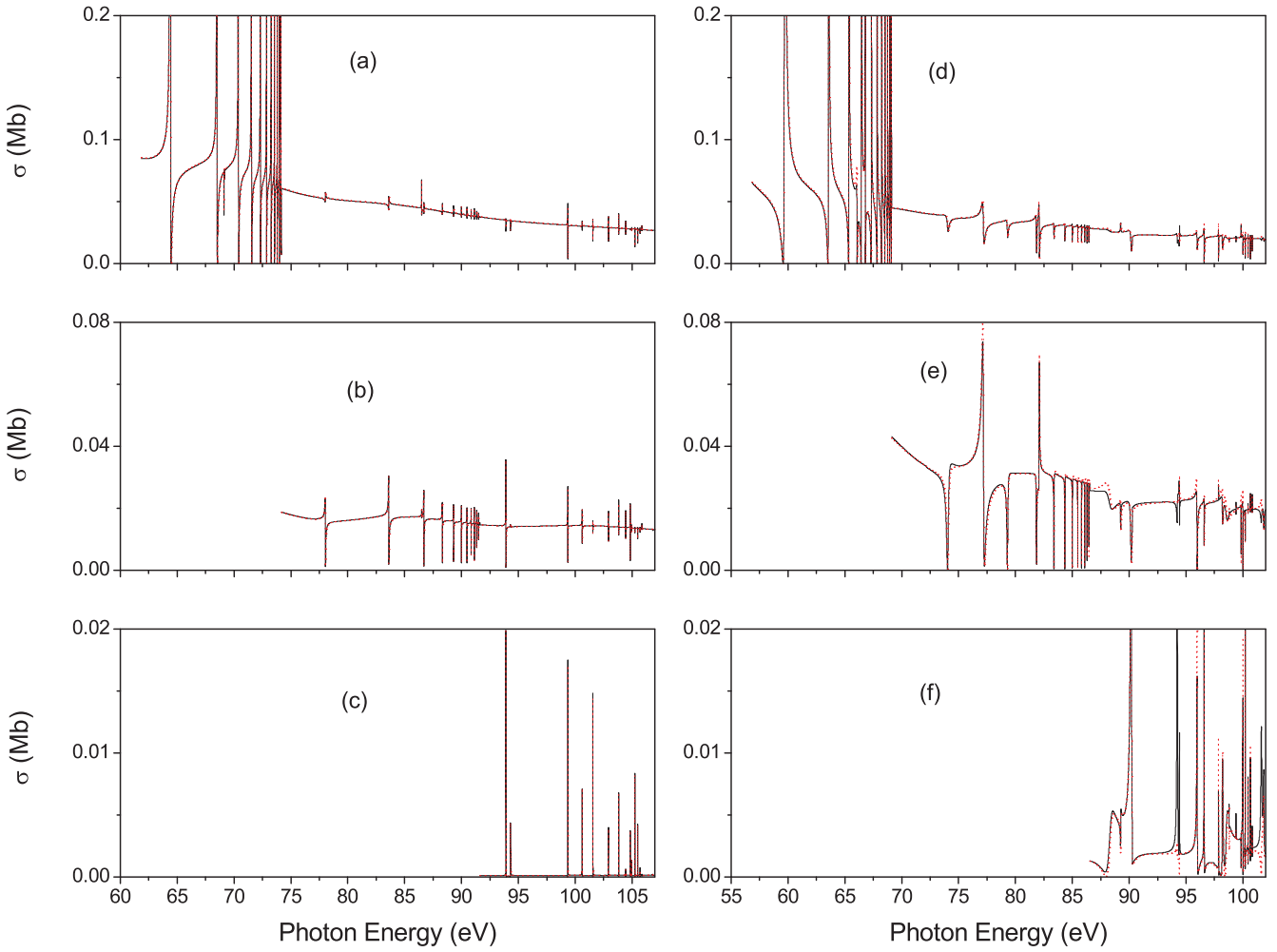


FIG. 3. (Color online) Partial photoionization cross sections for the processes $^{3,1}P^o \rightarrow {}^{3,1}S$ of the Mg-like $S^{4+}$ ion in the energy range up to the $S^{5+}$ $4s$ threshold limit as a function of the photon energy: (a) cross sections $\sigma_{3s\epsilon s}$ $^3S$, (b) cross sections $\sigma_{3p\epsilon p}$ $^3S$, (c) cross sections $\sigma_{3d\epsilon d}$ $^3S$, (d) cross sections $\sigma_{3s\epsilon s}$ $^1S$, (e) cross sections $\sigma_{3p\epsilon p}$ $^1S$, (f) cross sections $\sigma_{3d\epsilon d}$ $^1S$. The black solid and red dotted lines represent the present length and velocity results, respectively.

should tend to cancel each other. Furthermore, the resonance structure gets complex owing to the relatively small energy difference, ∼14 eV, between the $3d$ and $4s$ thresholds of $S^{5+}$. In addition, the intermixing among the resonances converging to the various $n = 3$ and $n = 4$ final ionic states is considerably greater for $S^{4+}$ than for Mg, $Al^+$, and $Si^{2+}$, resulting in a much more complex pattern of resonances for $S^{4+}$ photoionization. This occurs because the energy extent of the resonance series converging to each threshold increases with $Z$ much more rapidly than the splitting of the thresholds; in fact, as $Z \rightarrow \infty$, the $n = 3$ and $n = 4$ thresholds become degenerate [39]. This leads to the implication that the resonance situation becomes even more complex for the photoionization of the Mg-like $S^{4+}$ ion and higher members of the Mg isoelectronic sequence. Thus, it is evident from Table IV where the details of the resonant series converging on the $S^{5+}$ $3p$ threshold are given, and quite a number of anomalies are seen in the quantum defects and widths in virtually every series owing to interlopers from the lower members of the series converging to the $S^{5+}$ $3d$ and $4s$ thresholds. These interlopers affect several autoionizing Rydberg series, especially the $3p8s$ $^1P$ resonance, which shows an asymmetric behavior in shape compared with the other $3pns$ $^1P$ series. Furthermore, $3d4f$ $^1P$ resonance lies also below the $S^{5+}$ $3d$ threshold. Thus the resonances of the $3pns$ $^1P$ and $3pnd$ $^1P$ series represent the irregular patterns as shown in Fig. 2 and Table IV. Owing to these perturbations, the $3pns$ $^1P$ and $3pnd$ $^1P$ series converging to the $S^{5+}$ $3p$ threshold do not approach to a smooth regular behavior with approximately constant quantum defects even at $n = 10$, as seen in Table IV. If the quantum defects are nearly constant, it is expected that the widths decrease as $1/n^{*3}$ for the higher members of each of the resonance series.

### B. Photoionization from the excited $3s3p$ $^{3,1}P$ states of Mg-like $S^{4+}$ ion

In addition to the ground $3s^2$ $^1P$ state, the photoionization cross sections leading to the ionic $S^{5+}$ $3l$ states from the excited $3s3p$ $^{3,1}P$ states of the Mg-like $S^{4+}$ ion have been calculated in the energy region from the first ionization threshold up to the $S^{5+}$ $4s$ threshold limit. The photoionization processes from

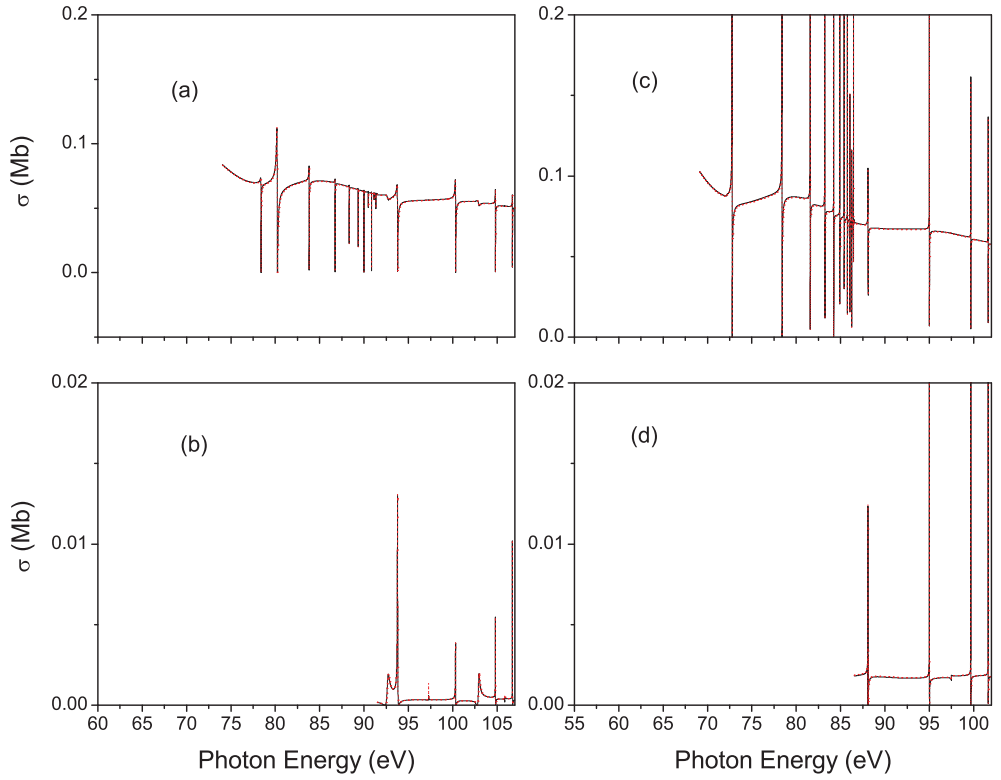


FIG. 4. (Color online) Partial photoionization cross sections for the processes $^{3,1}P^o \rightarrow {}^{3,1}P$ of the Mg-like $S^{4+}$ ion in the energy range up to the $S^{5+}$ $4s$ threshold limit as a function of the photon energy: (a) cross sections $\sigma_{3p\epsilon p}$ $^3P$, (b) cross sections $\sigma_{3d\epsilon d}$ $^3P$, (c) cross sections $\sigma_{3p\epsilon p}$ $^1P$, (d) cross sections $\sigma_{3d\epsilon d}$ $^1P$. The black solid and red dotted lines represent the present length and velocity results, respectively.

these excited states can leave the Mg-like $S^{4+}$ ion in either the photoionic $S^{5+}$ $3s$, $3p$, and $3d$ states. More specifically, along with the $3s\epsilon s$ $^{3,1}S$ and $3s\epsilon d$ $^{3,1}D$ channels below the $S^{5+}$ $3p$ threshold, the $3p\epsilon p$ $^{3,1}S$, $^{3,1}P$, $^{3,1}D$, and $3p\epsilon f$ $^{3,1}D$ channels open above the $S^{5+}$ $3p$ threshold. Thus, the $^{3,1}S$ and $^{3,1}D$ manifolds of the final continuum states can branch to either the $S^{5+}$ $3s$ or $S^{5+}$ $3p$ channels, but the $^{3,1}P$ manifold can lead only to the $S^{5+}$ $3p$ channel. These partial photoionization cross sections for the processes $3s3p$ $^{3,1}P \rightarrow 3l\epsilon l'$ $^{3,1}S$, $^{3,1}P$, $^{3,1}D$ of the Mg-like $S^{4+}$ ion are shown in Figs. 3–5. The length and velocity results are displayed by the black solid and red dotted curves, respectively.

It is noted that the $S^{5+}$ $3d$ production cross sections $\sigma_{3p\epsilon f}$ and $\sigma_{3d\epsilon s}$ for both triplet and singlet manifolds are also fundamentally different from the two lower $S^{5+}$ cross sections $\sigma_{3s\epsilon d}$ and $\sigma_{3p\epsilon p}$ in one very important way: Photoionization to the $S^{5+}$ $3s$ or $S^{5+}$ $3p$ is primarily single-electron transitions, predominantly $3s \rightarrow \epsilon d$ or $3p \rightarrow \epsilon p$, respectively. Photoionization to the $S^{5+}$ $3d$ state, on the other hand, requires a two-electron transition, i.e., photoionization plus excitation. This two-electron process is much less likely than a single-electron transition. As a result, it is expected that the background (nonresonant) cross section in this process will be extremely small. From Figs. 3–5, it is evident that this is indeed the case. On the scales shown, the nonresonant continuum cross sections are too small to appear. Thus, the strength of the $S^{5+}$ $3d$ cross sections, from both triplet and singlet states, is almost entirely due to resonances in the newly opened $S^{4+}$ $3d\epsilon l$ continua.

The associated channel cross sections for the photoionization of the excited $3s3p$ $^{3,1}P^o$ states of the $S^{4+}$ ion are obtained by adding the respective partial cross sections shown in Figs. 3–5, and these results are shown in Figs. 6(a)–6(f).

As shown in Figs. 3–6, the features of photoionization spectra for each of the triplet and singlet processes differ in several aspects. In the energy region below the $S^{5+}$ $3p$ threshold, there are three Rydberg series for each of the triplet and singlet manifolds, each converging to the $S^{5+}$ $3p$ threshold. The $^3P^o \rightarrow {}^3S$ cross section $\sigma_{3s\epsilon s}$ $^3S$, showing the $3pnp$ $^3S$ Rydberg series, is seen in Fig. 3(a); the $^3P^o \rightarrow {}^3D$ cross section $\sigma_{3s\epsilon d}$ $^3D$, showing the $3pnp$ $^3D$ and $3pnf$ $^3D$ Rydberg series is seen in Fig. 5(a). The analogous singlet cross sections, with the associated resonances, are presented in Figs. 3(d) and 5(f), respectively. Except for the resonances, it is clear that the cross sections are dominated by the $p \rightarrow d$ channel ($3s\epsilon d$), owing to a $(2L + 1)$ statistical weight factor that makes the $p \rightarrow d$ ($L = 2$) transition five times stronger than the $p \rightarrow s$ ($L = 0$) transition.

The autoionizing resonance series also shows very complex and irregular patterns. The autoionizing $3pnp$ $^{3,1}S$ resonance series converging to the ionic $S^{5+}$ $3p$, for instance, is perturbed by some interloper $3dnd$ $^{3,1}S$ series which converge to the $S^{5+}$ $3d$ threshold, as shown in Figs. 3(a) and 3(d), respectively. The lower members of these resonances have been studied in detail and their energy positions $E_r$, effective quantum numbers $n^*$, and widths $\Gamma_r$ are given in Tables V–VII.

It is noted that the $3pnp$ $^{3,1}S$ ($n \leqslant 5$) states are real bound states in our calculations, as indicated in Table V. Among

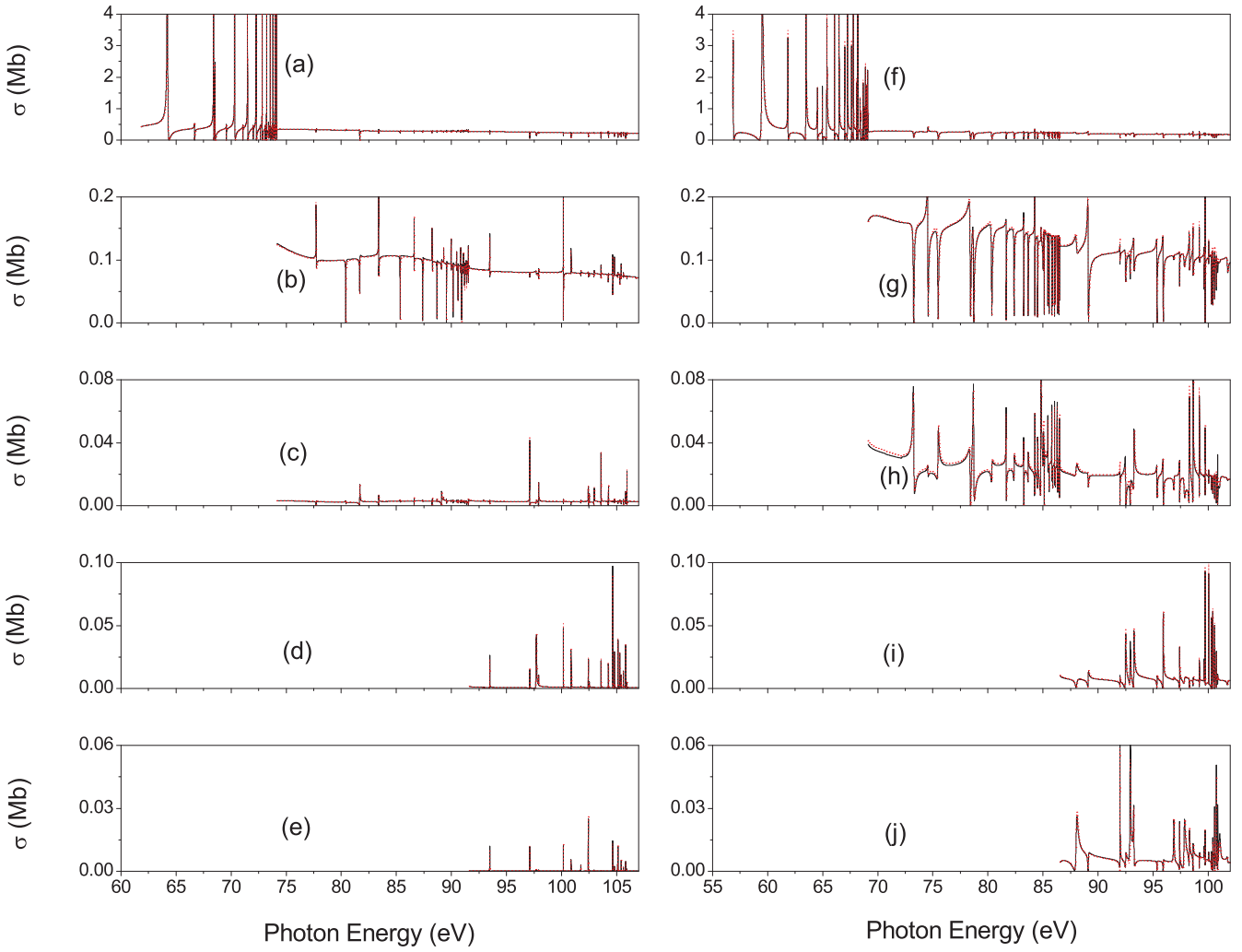


FIG. 5. (Color online) Partial photoionization cross sections for the processes $^{3,1}P^o \rightarrow {}^{3,1}D$ of the Mg-like $S^{4+}$ ion in the energy range up to the $S^{5+}$ $4s$ threshold limit as a function of the photon energy: (a) cross sections $\sigma_{3s\epsilon d}\ ^3D$, (b) cross sections $\sigma_{3p\epsilon p}\ ^3D$, (c) cross sections $\sigma_{3p\epsilon f}\ ^3D$, (d) cross sections $\sigma_{3d\epsilon s}\ ^3D$, (e) cross sections $\sigma_{3d\epsilon d}\ ^3D$, (f) cross sections $\sigma_{3s\epsilon d}\ ^1D$, (g) cross sections $\sigma_{3p\epsilon p}\ ^1D$, (h) cross sections $\sigma_{3p\epsilon f}\ ^1D$, (i) cross sections $\sigma_{3d\epsilon s}\ ^1D$, (j) cross sections $\sigma_{3d\epsilon d}\ ^3D$. The black solid and red dotted lines represent the present length and velocity results, respectively.

the $3pnp\ ^3S$ ($n \geqslant 6$) series, the $3p7p\ ^3S$ Rydberg resonance is depressed by the interloper $3d4d\ ^3S$ at 68.502 eV which converges to the $S^{5+}$ $3p$ threshold. Furthermore, the $3d7d\ ^3S$ resonance at 85.850 eV is affected by the interloper $4sns\ ^3S$ series which converges to the $S^{5+}$ $4s$ threshold. The $3p7p\ ^1S$ is also overlapped and depressed by the interloper $3d4d\ ^1S$ at 66.069 eV which converges to the $S^{5+}$ $3p$ threshold, and the $3dnd\ ^1S$ Rydberg series is affected by the $4sns\ ^1S$ series lying below the $S^{5+}$ $3d$ threshold. The presence of these several interlopers perturbs almost all the low members of resonance states substantially, as indicated by the deviations in quantum defects for both triplet and singlet manifolds, as listed in Table V.

The $3dnd\ ^{3,1}P$ ($n \leqslant 4$) states are real bound states in our calculations, as indicated in Table VI. The $3d6d\ ^3P$ Rydberg resonance is depressed by the interloper $4p5p\ ^3P$ at 80.216 eV, which converges to the $S^{5+}$ $4p$ threshold for the triplet manifold, while the $3d7d\ ^1P$ Rydberg resonance is depressed by the interloper $4p5p\ ^1P$ at 78.407 eV, which converges to the $S^{5+}$ $4p$ threshold for the singlet manifold. Owing to the effect of some interlopers $4lnl'\ ^{3,1}P$ lying below the $S^{5+}$ $3d$ threshold, the $3dnd\ ^{3,1}P$ series does not display regular behavior with approximately constant quantum defects even at $n = 10$, as seen in Table VI.

As for the photoionization processes of $^{3,1}P^o \rightarrow {}^{3,1}D$, the $3pnp\ ^{3,1}D$ ($n \leqslant 5$) states are also real bound states in our calculations, as indicated in Table VII. The $3pnp\ ^3S$ ($n \geqslant 6$) Rydberg series are seriously affected by some interlopers lying below the $S^{5+}$ $3p$ threshold. For instance, interloper $4s4d\ ^3D$ is located at 84.808 eV between the $3d7s\ ^3D$ and $3d7d\ ^3D$ Rydberg series. Another interloper $4s5d\ ^3D$ is located at 89.244 eV between the $3d10s\ ^3D$ and $3d10d\ ^3D$ Rydberg series. The $3p7p\ ^3D$ resonance appears to be pushed to a higher energy by the interaction with the interlopers $3d4s\ ^3D$ at 68.489 eV and $3d4d\ ^3D$ at 68.512 eV, and the $3p8p\ ^3P$ resonance is also affected by those interlopers. The $3p9f\ ^3D$ and $3p10f\ ^3D$ resonances appear to have a similar influence as shown in Table VII.

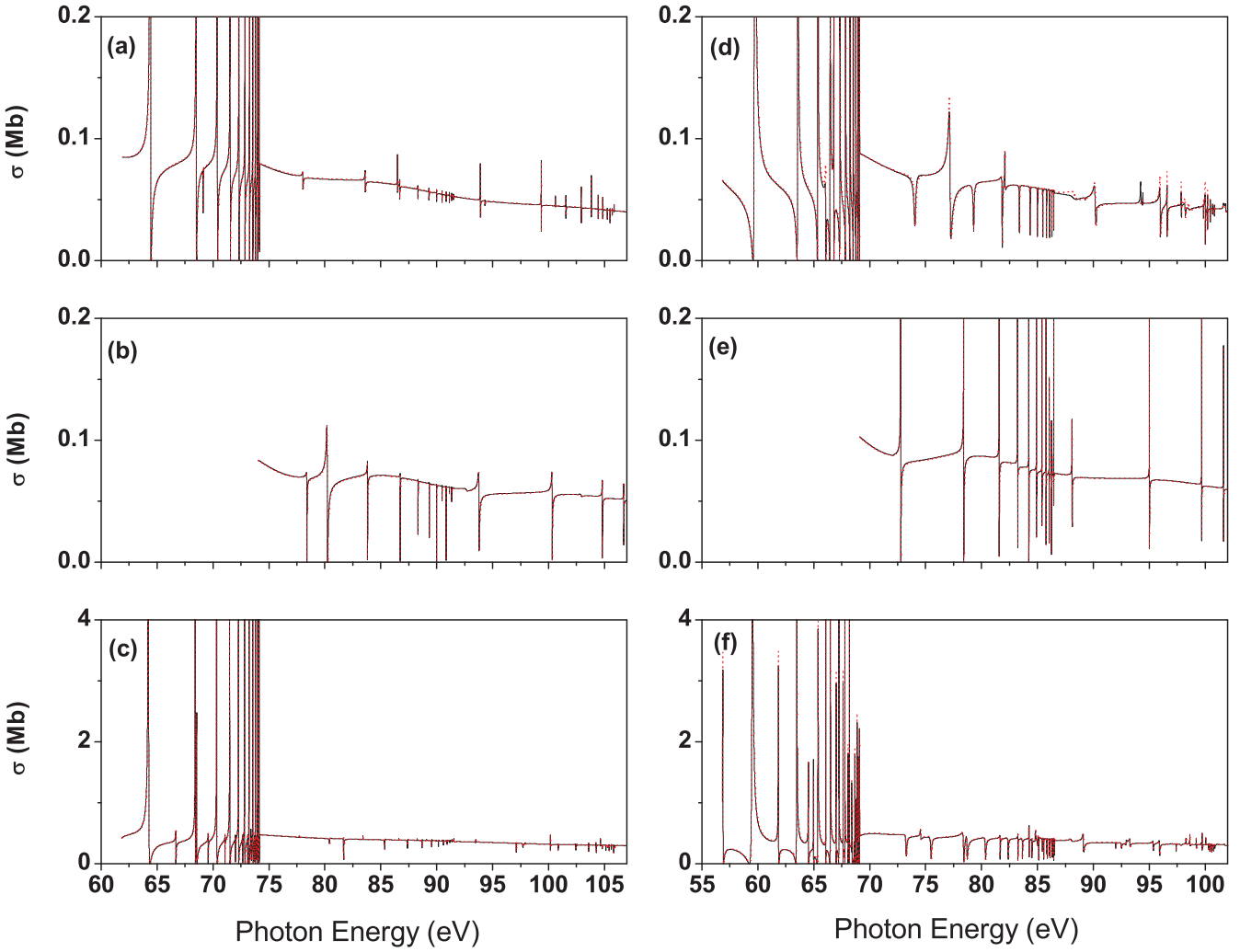


FIG. 6. (Color online) Photoionization cross sections for the processes $^{3,1}P^o \rightarrow {}^{3,1}S$, $^{3,1}P$, $^{3,1}D$ of the Mg-like $S^{4+}$ ion in the energy range up to the $S^{5+}$ $4s$ threshold limit as a function of the photon energy: (a) cross sections for the $^3P^o \rightarrow {}^3S$ process, (b) cross sections for the $^3P^o \rightarrow {}^3P$ process, (c) cross sections for the $^3P^o \rightarrow {}^3D$ process, (d) cross sections for the $^1P^o \rightarrow {}^1S$ process, (e) cross sections for the $^1P^o \rightarrow {}^1P$ process, (f) cross sections for the $^1P^o \rightarrow {}^1D$ process. The black solid and red dotted lines represent the present length and velocity results, respectively.

One of the interlopers $3d^2\ ^1D$ is located at 59.548 eV and another interloper $3d4s\ ^1D$ is located at 64.987 eV between $3p78\ ^1D$ and $3p9f\ ^1D$. Because of the effects of these interlopers converging to the $S^{5+}$ $3d$ or $4l$ thresholds, there are considerable perturbations at the $3pnp\ ^1D$ and $3pnf\ ^1D$ Rydberg series. The $3d4s\ ^1D$ interloper almost overlaps with the $3p7p\ ^1D$ resonance. The $4s4d\ ^1D$ state at 68.666 eV just above the $3d5s\ ^1D$ resonance is an interloper.

Thus, the photoionization spectra show very complex and irregular patterns. These irregularities are due to perturbations from other interlopers which we have not analyzed in detail but are still included in the calculation. These interlopers converging to the $S^{5+}$ $3d$ or $4l$ thresholds are located at 75.509, 80.336, 81.598, 82.358, 83.235, and 83.796 eV in our calculations.

The total photoionization cross sections for the photoionization of the excited $3s3p\ ^{3,1}P$ states of ionic $S^{4+}$ are obtained by adding the respective channel cross sections shown in Fig. 6. The present and OP results [21] for the total photoionization cross sections of the excited $3s3p\ ^{3,1}P$ states are shown in Figs. 7(a) and 7(b), respectively. Our results show overall agreement with the OP results. However, some discrepancies are found between the two different results for both triplet and singlet cases, as shown in Fig. 7.

### C. Convoluted cross sections for photoionization of Mg-like $S^{4+}$ ion

The convoluted cross sections in the range of 56–93 eV for the photoionization of ground $3s^2\ ^1S$ and excited $3s3p\ ^{3,1}P$ states for the Mg-like $S^{4+}$ ion are shown in Figs. 8(a)–8(c). Though there are no available experiments for a Mg-like $S^{4+}$ ion, the theoretical spectra have been convoluted with Gaussians of 250 meV [full width at half maximum (FWHM)] for future experiments, since the recent experiments for the Be-like $N^{2+}$, $O^{3+}$, and $F^{4+}$ ions [31] have been performed with energy resolutions of 100, 250, and 500 meV, respectively. The major Rydberg series exhibited in these cross sections are the $3s3p\ ^3P \rightarrow 3pnp\ ^3S$, $^3P$, and

TABLE V. Effective quantum number ($n^*$), position ($E_r$ in eV), and width ($\Gamma_r$ in eV) of resonances converging to the $S^{5+}$ $3l$ thresholds, which are owing to the photoionization processes $^{3,1}P^o \rightarrow {}^{3,1}S$.

| $^3S$ | | | | $^1S$ | | | |
|---|---|---|---|---|---|---|---|
| $3pnp$ | $n^*$ | $E_r$ | $\Gamma_r$ | $3pnp$ | $n^*$ | $E_r$ | $\Gamma_r$ |
| 6 | 5.628 | 64.396 | 0.051 | 6 | 5.729 | 59.713 | 0.124 |
| 7 | | | | | | | |
| 8 | 7.536 | 69.146 | 0.002 | 8 | 7.228 | 63.568 | 0.063 |
| 9 | 8.462 | 70.386 | 0.027 | 9 | 8.492 | 65.362 | 0.032 |
| 10 | 9.713 | 71.530 | 0.019 | 10 | 9.693 | 66.458 | 0.118 |
| $3dnd$ | $n^*$ | $E_r$ | $\Gamma_r$ | $3dnd$ | $n^*$ | $E_r$ | $\Gamma_r$ |
| 4 | 3.758 | 68.502 | 0.034 | 4 | 3.982 | 66.071 | 0.133 |
| 5 | 4.811 | 78.031 | 0.090 | 5 | 4.705 | 72.160 | |
| 6 | 6.107 | 83.606 | 0.073 | 6 | 5.734 | 77.182 | 0.438 |
| 7 | 7.033 | 85.850 | | 7 | 6.429 | 79.296 | 0.317 |
| 8 | 7.507 | 86.690 | 0.014 | 8 | 7.737 | 81.845 | 0.144 |
| 9 | 8.776 | 88.309 | 0.012 | 9 | 9.065 | 83.387 | 0.092 |
| 10 | 9.985 | 89.314 | 0.010 | 10 | 10.339 | 84.345 | 0.018 |

TABLE VI. Effective quantum number ($n^*$), position ($E_r$ in eV), and width ($\Gamma_r$ in eV) of resonances converging to the $S^{5+}$ $3l$ thresholds, which are owing to the photoionization processes $^{3,1}P^o \rightarrow {}^{3,1}P$.

| $^3P$ | | | | $^1P$ | | | |
|---|---|---|---|---|---|---|---|
| $3dnd$ | $n^*$ | $E_r$ | $\Gamma_r$ | $3dnd$ | $n^*$ | $E_r$ | $\Gamma_r$ |
| 5 | 4.896 | 78.393 | 0.059 | 5 | 4.802 | 72.776 | 0.021 |
| 6 | | | | 6 | 5.980 | 78.015 | |
| 7 | 6.229 | 83.817 | 0.037 | 7 | | | |
| 8 | 7.631 | 86.743 | 0.015 | 8 | 7.566 | 81.584 | 0.009 |
| 9 | 8.949 | 88.336 | 0.004 | 9 | 8.890 | 83.222 | |
| 10 | 9.738 | 88.997 | | 10 | 9.937 | 84.082 | |

$^3D$ transitions, and $3s^2\ {}^1S \rightarrow 3pns\ {}^1P$ transitions from the ground state. The assignments of the resonances have been given in Tables V–VII. As shown in Fig. 8, especially it is expected that the resonance effects for photoionization of the $3s3p\ {}^3P$ state are considerable in the measurement of the absolute cross sections, since the resonance structures of the ground $3s^2\ {}^1S$ state are relatively not strong.

TABLE VII. Effective quantum number ($n^*$), position ($E_r$ in eV), and width ($\Gamma_r$ in eV) of resonances converging to the $S^{5+}$ $3l$ thresholds, which are owing to the photoionization processes $^{3,1}P^o \rightarrow {}^{3,1}D$.

| $^3D$ | | | | $^1D$ | | | |
|---|---|---|---|---|---|---|---|
| $3pnp$ | $n^*$ | $E_r$ | $\Gamma_r$ | $3pnp$ | $n^*$ | $E_r$ | $\Gamma_r$ |
| 6 | 5.582 | 64.220 | 0.199 | 6 | 5.671 | 59.503 | 0.413 |
| 7 | 7.111 | 68.409 | 0.028 | 7 | 7.179 | 63.479 | 0.094 |
| 8 | 7.179 | 68.536 | 0.061 | 8 | 8.168 | 64.980 | 0.026 |
| 9 | 8.412 | 70.328 | 0.064 | 9 | 9.217 | 66.075 | 0.004 |
| 10 | 9.569 | 71.490 | 0.046 | 10 | 10.493 | 66.989 | 0.002 |
| $3pnf$ | $n^*$ | $E_r$ | $\Gamma_r$ | $3pnf$ | $n^*$ | $E_r$ | $\Gamma_r$ |
| 7 | 6.342 | 66.678 | 0.058 | 7 | 6.427 | 61.842 | 0.061 |
| 8 | 7.816 | 69.568 | 0.022 | 8 | 7.824 | 64.522 | 0.059 |
| 9 | 9.143 | 71.067 | 0.016 | 9 | 8.501 | 65.371 | 0.121 |
| 10 | 10.423 | 72.005 | 0.013 | 10 | 9.719 | 66.478 | 0.052 |
| $3dns$ | $n^*$ | $E_r$ | $\Gamma_r$ | $3dns$ | $n^*$ | $E_r$ | $\Gamma_r$ |
| 4 | 3.757 | 68.489 | | 4 | 3.762 | 63.493 | |
| 5 | 4.347 | 74.579 | | 5 | 4.259 | 68.770 | 0.062 |
| 6 | 5.286 | 80.408 | 0.085 | 6 | 5.313 | 75.476 | 0.306 |
| 7 | 6.083 | 83.391 | 0.028 | 7 | 6.207 | 78.698 | 0.234 |
| 8 | 7.549 | 86,615 | 0.011 | 8 | 7.615 | 81.661 | 0.056 |
| 9 | 8.871 | 88.261 | 0.008 | 9 | 8.926 | 83.257 | 0.027 |
| 10 | 9.882 | 89.100 | 0.094 | 10 | 9.371 | 83.653 | 0.085 |
| $3dnd$ | $n^*$ | $E_r$ | $\Gamma_r$ | $3dnd$ | $n^*$ | $E_r$ | $\Gamma_r$ |
| 4 | 3.759 | 68.512 | 0.145 | 4 | 3.884 | 64.987 | 0.003 |
| 5 | 4.784 | 77.722 | 0.039 | 5 | 4.494 | 70.687 | |
| 6 | 5.584 | 81.674 | 0.071 | 6 | 6.105 | 78.399 | 0.283 |
| 7 | 6.856 | 85.346 | 0.057 | 7 | 6.883 | 80.347 | 0.260 |
| 8 | 8.100 | 87.399 | 0.036 | 8 | 8.125 | 82.374 | 0.148 |
| 9 | 9.350 | 88.692 | 0.021 | 9 | 9.271 | 83.569 | |
| 10 | 10.161 | 89.289 | 0.009 | 10 | 10.176 | 84.241 | 0.015 |

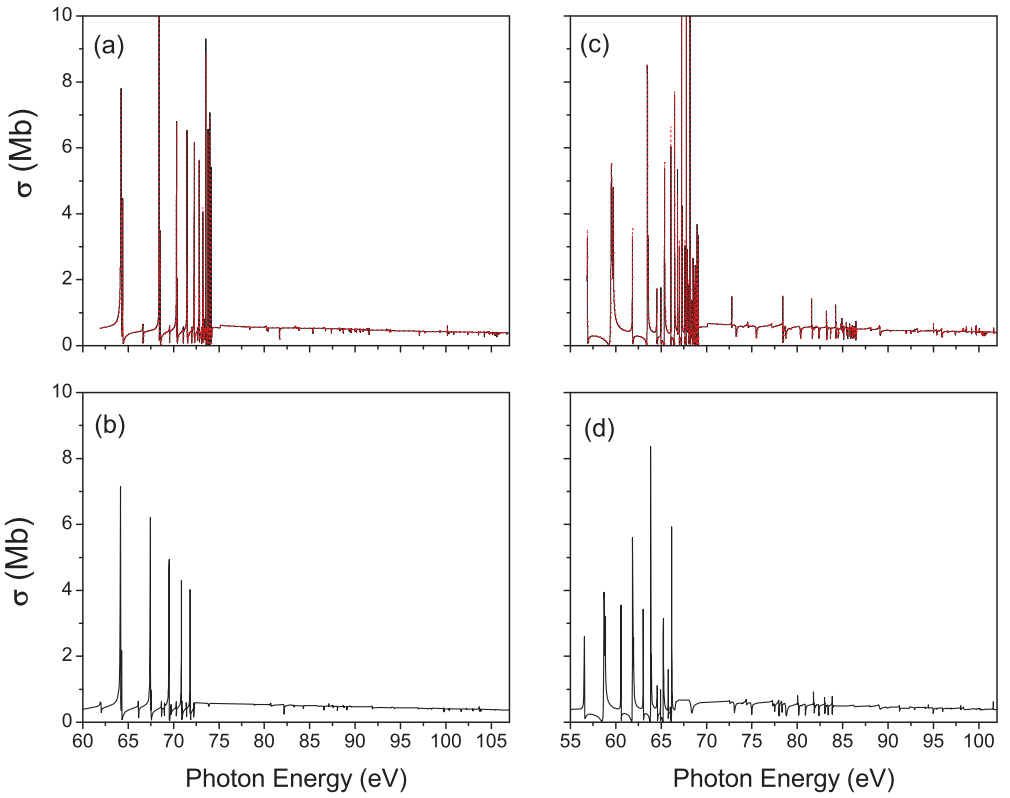


FIG. 7. (Color online) Total photoionization cross sections for the excited $3s3p\ ^{3,1}P$ states of the Mg-like $S^{4+}$ ion as a function of photon energy. (a) Present results for $^3P$: black solid curve, present length; red dashed, present velocity. (b) OP results for $^3P$. (c) Present results for $^1P$: black solid curve, present length; red dashed, present velocity. (d) OP result for $^1P$.

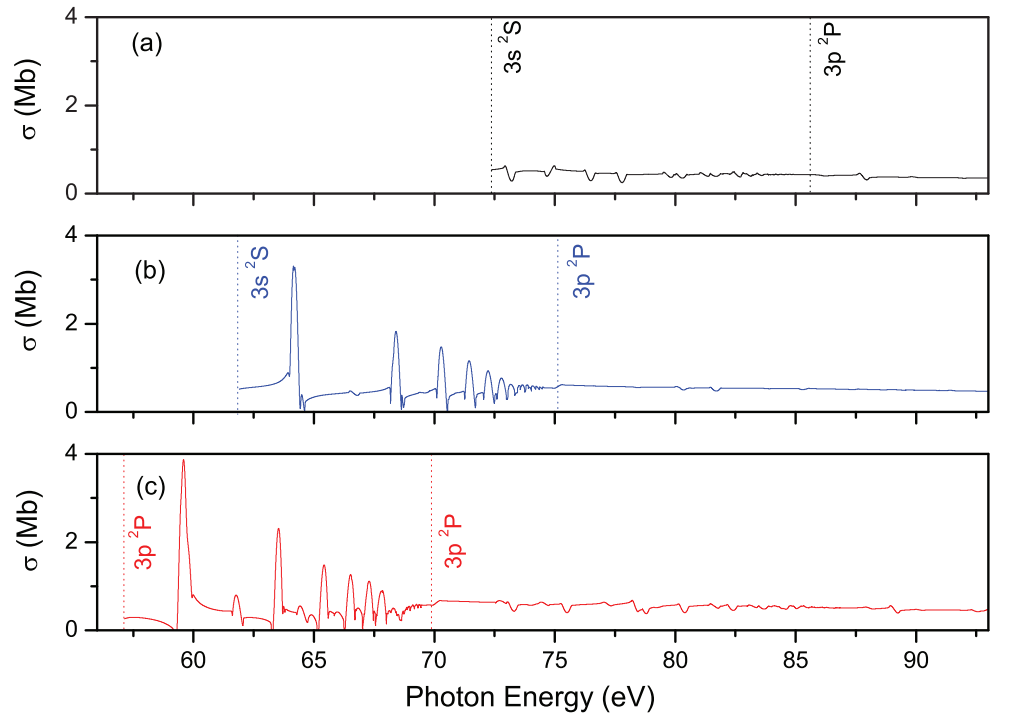


FIG. 8. (Color online) The convoluted photoionization cross sections in the energy range 56–93 eV as a function of the photon energy: (a) Convoluted cross sections for the ground state, (b) convoluted cross sections for the excited $3s3p\ ^3P$ state, and (c) convoluted cross sections for the excited $3s3p\ ^1P$ state. The present results have convoluted with a Gaussian profile assuming a broadening of 250 meV (FWHM). The vertical dotted lines represent the thresholds for the ground $3s^2\ ^1S$ and $3s3p\ ^{3,1}P$ states, respectively.

## IV. CONCLUSIONS

The photoionization of the Mg-like $S^{4+}$ ion has been studied in the energy range from the $S^{5+}$ $3s$ to the $S^{5+}$ $4s$ threshold, using a rather efficient noniterative eigenchannel $R$-matrix method which is different from the widely used iterative $R$-matrix approach. The calculational results are compared with previous theoretical OP results with quite reasonable agreement.

It is noted that for most Rydberg series of autoionizing resonances converging to the $S^{5+}$ $3d$ and $4s$ thresholds, many members lie below the $S^{5+}$ $3p$ threshold and these interlopers act as perturbers; this occurs since the energy differences between the $S^{5+}$ $3l$ thresholds are very small. In addition, the energy scale increases roughly as $Z^2$ by the hydrogenic energy scaling. However, the energy separation between $nl$ and $nl'$ increases roughly as $Z$ along the isoelectronic sequences. Thus, the energy extent of the resonance series converging to each threshold increases with $Z$ much more rapidly than the splitting of the thresholds, as mentioned above. This leads to the implication that the resonance situation becomes even more complex for the photoionization of the Mg-like $S^{4+}$ ion and higher members of the Mg isoelectronic sequence. However, using the ideas of eigenphase sum gradients, a detailed analysis and identification of the low-lying autoionizing levels is presented, which is a difficult process due to the overlap of the various series converging to different thresholds.

Since there is no previous experiment for the $S^{4+}$ ion, experimental studies for this ion would be required to confirm our understanding of the physics of these photoionization processes. This work will be extended in several directions: First, the photoionization of the Mg-like $Cl^{5+}$ and $Ar^{6+}$ ions will be considered, both ground and excited states, to understand the evolution of the resonances for the Mg isoelectronic sequence and to provide accurate data on these systems for astrophysical as well as industrial plasma databases.

## ACKNOWLEDGMENT

This work was supported by the Korean Ministry of Science, ICT and Future Planning (MSIP).

[1] M. Spite, E. Caffau, S. M. Andrievsky *et al.*, Astron. Astrophys. **528**, 8 (2011).
[2] G. N. Bates and P. L. Altic, J. Phys. B **6**, 653 (1973).
[3] J. Dubau and J. Wells, J. Phys. B **6**, L31 (1973).
[4] C. H. Greene, Phys. Rev. A **23**, 661 (1981).
[5] P. F. O'Mahony and C. H. Greene, Phys. Rev. A **31**, 250 (1985).
[6] V. Radojevic and W. R. Johnson, Phys. Rev. A **31**, 2991 (1985).
[7] R. Moccia and P. Spizzo, J. Phys. B **21**, 1133 (1988).
[8] Z. Altun, Phys. Rev. A **40**, 4968 (1989).
[9] K. Butler, C. Mendoza, and C. J. Zeippen, Mon. Not. R. Astron. Soc. **209**, 343 (1984).
[10] K. Butler, C. Mendoza, and C. J. Zeippen, Mon. Not. R. Astron. Soc. **213**, 345 (1985).
[11] K. Butler, C. Mendoza, and C. J. Zeippen, J. Phys. B **26**, 4409 (1993).
[12] H.-C. Chi and K.-N. Huang, Phys. Rev. A **50**, 392 (1994).
[13] H.-C. Chi, Phys. Rev. A **56**, 4118 (1997).
[14] D.-S. Kim and S. S. Tayal, J. Phys. B **33**, 3235 (2000).
[15] D.-S. Kim, J. Phys. B **34**, 2615 (2001).
[16] D.-S. Kim and Y. S. Kim, J. Phys. Soc. Jpn. **76**, 014302 (2007).
[17] D.-S. Kim and Y. S. Kim, J. Phys. B **41**, 165002 (2008).
[18] D.-S. Kim and F. Koike, J. Phys. Soc. Jpn. **77**, 124302 (2008).
[19] M. Seaton, J. Phys. B **20**, 6363 (1987).
[20] OP Team, *The Opacity Project* (Institute of Physics Publishing, Bristol, UK, 1995), Vol. 1.
[21] http://cdsweb.u-strasbg.fr/topbase/topbase.html.
[22] G. Mehlman-Balloffet and J. M. Esteva, Astrophys. J. **157**, 945 (1969).
[23] J. M. Preses, C. E. Burkhardt, W. P. Garver, and J. J. Leventhal, Phys. Rev. A **29**, 985 (1984).
[24] W. Fiedler, C. Kortenkamp, and P. Zimmermann, Phys. Rev. A **36**, 384 (1987).
[25] G. W. Schinn, C. J. Dai, and T. F. Gallagher, Phys. Rev. A **43**, 2316 (1991).
[26] R. Wehlitz, D. Lukić, and P. N. Juranić, J. Phys. B **40**, 2385 (2007).
[27] J. B. West, T. Andersen, R. L. Brooks, F. Folkmann, H. Kjeldsen, and H. Knudsen, Phys. Rev. A **63**, 052719 (2001).
[28] M. H. Sayyad, E. T. Kennedy, L. Kiernan, J.-P. Mosnier, and J. T. Costello, J. Phys. B **28**, 1715 (1995).
[29] S. Schippers, A. Müller, B. M. McLaughlin, A. Aguilar, C. Cisneros, E. D. Emmons, M. F. Gharaibeh, and R. A. Phaneuf, J. Phys. B **36**, 3371 (2003).
[30] A. Müller, R. A. Phaneuf, A. Aguilar, M. F. Gharaibeh, A. S. Schlachter, I. Alvarez, C. Cisneros, G. Hinojosa, and B. M. McLaughlin, J. Phys. B **35**, L137 (2002).
[31] J.-M. Bizau, J.-P. Champeaux, D. Cubaynes, F. J. Wuilleumier, F. Folkmann, T. S. Jacobsen, F. Penent, C. Blancard, and H. Kjeldsen, Astron. Astrophys. **439**, 387 (2005).
[32] I. Orban, E. Lindroth, P. Glans, and R. Schuch, J. Phys. B **40**, 1063 (2007).
[33] A. M. Covington, A. Aguilar, I. R. Covington, M. Gharaibeh, C. A. Shirley, R. A. Phaneuf, I. Álvarez, C. Cisneros, G. Hinojosa, J. D. Bozek, I. Dominguez, M. M. Sant'Anna, A. S. Schlachter, N. Berrah, S. N. Nahar, and B. M. McLaughlin, Phys. Rev. Lett. **87**, 243002 (2001).
[34] F. Robicheaux, Phys. Rev. A **43**, 5946 (1991).
[35] M. Aymar, C. H. Greene, and E. Luc-Koenig, Rev. Mod. Phys. **68**, 1015 (1996).
[36] W. R. Johnson, D. Kolb, and K.-N. Huang, At. Data Nucl. Data Tables **28**, 333 (1983).
[37] C. H. Greene and C. Jungen, Adv. At. Mol. Phys. **21**, 51 (1985).
[38] http://www.nist.gov/pml/data/asd.cfm.
[39] W.-C. Chu, H.-L. Zhou, A. Hibbert, and S. T. Manson, J. Phys. B **42**, 205003 (2009).